Self-similar solutions for a nonlinear radiation diffusion equation

Josselin Garnier
Laboratoire de Probabilités et Modèles Aléatoires & Laboratoire Jacques-Louis Lions, Université Paris VII, 2 Place Jussieu, 75251 Paris Cedex 5, France

Guy Malinié, Yves Saillard, and Catherine Cherfils-Clérouin
Commissariat à l'Energie Atomique, Direction des Applications Militaires, BP12, 91680 Bruyères le Châtel, France

(Received 22 June 2006; accepted 15 August 2006; published online 27 September 2006)

This paper considers the hydrodynamic equations with nonlinear conduction when the internal energy and the opacity have power-law dependences in the density and in the temperature. This system models the situation in which a dense solid is brought into contact with a thermal bath. It supports self-similar solutions that depend on the surface temperature. The self-similar solution can exhibit a shock wave followed by an ablation front if the surface temperature does not increase too fast in time, but it can exhibit a heat front followed by an isothermal shock otherwise. These flows are carefully studied in order to clarify the role of the initial solid density in the energy absorption and the ablation process. Comparisons with numerical simulations show excellent agreement.
 [DOI: 10.1063/1.2350167]

I. INTRODUCTION

Radiation heat waves play important roles in plasma physics, and in particular in inertial confinement fusion (ICF). In indirectly driven ICF experiments, laser beams illuminate the inner wall of a high-Z cavity, which is designed to convert the laser energy into x rays. It is therefore important to understand how the laser energy is absorbed by the hohlraum inner wall. As shown by Marshak, it is possible to obtain exact solutions for the radiative flow in some special configurations.[1] These solutions are of particular interest for ICF.[2] Self-similar solutions were obtained in Refs. 3–5, in particular, in the limit where the solid wall can be considered as infinitely dense.[6–9] Reasonable agreement was found with experimental results.[10] Recently, Hammer and Rosen[11] proposed solutions based on a perturbation theory using the small parameter $\varepsilon=\beta/(4+\alpha)$, where the internal energy varies as T^{β} and the opacity varies as $T^{-\alpha}$. Rosen and Hammer[12] followed that study with a new development, showing that absorbed energy in a low density (foam) wall can be reduced compared to the infinitely dense limit.

In this paper, we study the radiation diffusion equation in different regimes. We consider the situation wherein a dense body is suddenly brought into contact with a thermal bath. A steep temperature gradient is set up, which generates a diffusive heat wave. Simultaneously a high pressure is created, which induces hydrodynamic expansion. The main goal of this paper is to obtain exact analytic expressions for the physically relevant quantities, such as the position of the heat front, the absorbed energy, and the ablation pressure. The main application we have in mind is indirectly driven ICF, with radiation heat conduction, but the results of the paper can also be applied to other situations with nonlinear heat conduction, such as electronic heat conduction.

The physics of the problem is rather classical and the phenomenology can be found, for instance, in Ref. 14 (Chap. X, Sec. 8). As described there, the heating of the body can be divided into two main phases. First, a supersonic heat wave propagates into the undisturbed material. As the thickness of the heated material increases, the velocity of the heat wave decreases. Simultaneously, hydrodynamic expansion of the heated material into the vacuum begins. This supersonic regime is analyzed in Sec. II. This regime ends up when the front of heat wave has slowed down to approximately the speed of sound. It is then overtaken by a shock wave. The subsequent phase (the subsonic regime) where the heat wave is preceded by a shock wave and accompanied by hydrodynamic expansion is analyzed in Sec. III.

The *supersonic regime* addresses the first time steps, when the speed of sound is smaller than the velocity of the heat front. This regime is valid during the time interval $t_{\mathrm{DA}}\ll t<t_{\mathrm{HS}}$, where t_{DA} is the time that ensures the validity of the diffusion approximation, and t_{HS} is the hydrodynamic separation time. For a fixed time t and surface temperature T_{S0}, the supersonic regime can be observed if the initial density of the body is smaller than the critical value $\rho_{\mathrm{HS}}(t,T_{S0})$ [Eq. (24)], and larger than a very small value ρ_{DA} that ensures the validity of the diffusion approximation. In the supersonic regime, the absorbed energy depends on the initial density. By taking into account the propagation of the rarefaction wave behind the heat front, we can get an analytic formula for the absorbed energy as a function of time, initial density, and surface temperature. For a given time t and surface temperature T_{S0}, this formula presents a minimum $E_{\min}(t,T_{S0})$ [Eq. (28)] achieved for the optimum density $\rho_{\min}(t,T_{S0})$ [Eq. (27)].

The *subsonic regime* addresses the case in which the density of the body is much larger than the typical ablated material density. This regime is valid during the time interval $t_{\mathrm{HS}}\ll t\ll t_{\mathrm{rad}}$, where t_{rad} is the time at which the radiation pressure and energy become non-negligible. For fixed time t and surface temperature T_{S0}, the subsonic regime can be observed if the initial density of the body is larger than the

critical value $\rho_{\mathrm{HS}}(t,T_{S0})$. In this regime, the absorbed energy $E_{\mathrm{sub}}(t,T_{S0})$ [Eq. (43)] depends on time and surface temperature, but it is independent of the initial density. It turns out that E_{sub} is larger than E_{min} by a factor that is independent of t and T_{S0}. This result is important for ICF applications, as it means that there exists an *optimum wall density* for minimizing the energy lost by ablating the wall. This result was first derived in Ref. 12 via a relatively simple approach, and in our paper is re-derived in a more rigorous and general way.

The phenomenology that we have just described is observed if the imposed surface temperature is constant or does not increase too steeply with time. Otherwise, the phenomenology is reversed: we observe in the early time steps a shock wave followed by a heat front, but the heat front eventually overtakes the shock wave. This regime deserves a separate study that we will not perform in this paper, because it is not a regime that is interesting for the applications we have in mind. However, there exists a special regime, just between the two general regimes, when the surface temperature increases in time with the *critical power law*. This regime is characterized by a globally self-similar flow. It is actually very rich, and it can exhibit different qualitative behaviors depending on the initial solid density. If the density is low, then a heat front followed by an isothermal shock is generated at time 0. If the density is high, then a shock wave followed by an ablation front is generated, and these structures are preserved in time up to an expansion. These flows can be computed analytically and they are described in detail in Sec. IV.

Main hypotheses. We use the same notation as Ref. 11. We assume that the internal energy per unit mass e and the Rosseland mean opacity K have power-law dependences with respect to the density ρ and the temperature T:

$$e = fT^{\beta}\rho^{-\mu}, \quad \frac{1}{K} = gT^{\alpha}\rho^{-\lambda}, \tag{1}$$

where f and g are two dimensional constants and β, μ, α, and λ are given exponents. The equation of state is

$$P = r\rho e,$$

where P is the pressure and $r>0$ is a dimensionless constant ($1+r$ is the adiabatic exponent). If, in addition, the surface temperature has a power-law dependence in time, then the flows are self-similar in the supersonic regime and in the subsonic regime. The work by Hammer and Rosen[11] is based on asymptotic expansions with respect to the parameter $\varepsilon = \beta/(4+\alpha)$, which allows them to obtain analytic expressions of the first terms of the expansions for a large class of boundary conditions. This method is justified by the numerical values corresponding to gold in the temperature range 100–200 eV:

$$\alpha = 1.5, \quad \beta = 1.6, \quad \mu = 0.14, \quad \lambda = 0.2, \quad r = 0.25, \tag{2}$$

so that $\varepsilon \simeq 0.291$. In our paper we propose a method that is based on a simple eigenvalue problem that can be solved by integrating numerically a closed system of ordinary differential equations. This procedure is straightforward and allows us to obtain time and space profiles for the physically relevant quantities, whatever the values of the parameters α and β are.

Remark about the thermodynamic consistency. For a reversible system, the first and second laws of thermodynamics require that the internal energy satisfies the exact differential equation

$$de = TdS - PdV = TdS + \frac{P}{\rho^2}d\rho,$$

where S is the entropy and V is the specific volume. Taking into account the identities $e=fT^{\beta}\rho^{-\mu}$ and $P=r\rho e$, we get

$$dS = f\beta T^{\beta-2}\rho^{-\mu}dT - f(\mu+r)T^{\beta-1}\rho^{-\mu-1}d\rho.$$

This must be an exact differential equation, which imposes

$$\frac{\partial}{\partial\rho}(f\beta T^{\beta-2}\rho^{-\mu}) = \frac{\partial}{\partial T}[-f(\mu+r)T^{\beta-1}\rho^{-\mu-1}].$$

This equation is fulfilled if $\mu\beta=(\mu+r)(\beta-1)$, i.e., $\mu=r(\beta-1)$. Note that the thermodynamic consistency is almost satisfied with the numerical values (2) given in Ref. 11.

II. SUPERSONIC WAVES

A. The nonlinear heat equation

We consider the situation in which the right half-space $x>0$ is filled by a solid body with density ρ_0, while the other half-space $x<0$ is empty. At time $t=0$, the dense body is brought into contact with a thermal bath whose temperature is $T_S(t)$.

In the absence of hydrodynamic motion, the equation for supersonic radiative transport in one dimension is

$$\rho\frac{\partial e}{\partial t} = \frac{4}{3}\frac{\partial}{\partial x}\frac{1}{K\rho}\frac{\partial\sigma T^4}{\partial x},$$

where the parameter σ is the Stefan-Boltzmann constant. Substituting (1) into it and taking into account the fact that $\rho=\mathrm{const}=\rho_0$, we obtain the nonlinear heat equation

$$\frac{\partial T^{\beta}}{\partial t} = C\frac{\partial^2 T^{4+\alpha}}{\partial x^2},$$

where C is the parameter

$$C = \frac{16}{12+3\alpha}\frac{g\sigma}{f\rho_0^{2-\mu+\lambda}}.$$

Introducing $\varepsilon=\beta/(4+\alpha)$ and $\zeta=T^{4+\alpha}$, the heat equation takes the form

$$\frac{\partial\zeta^{\varepsilon}}{\partial t} = C\frac{\partial^2\zeta}{\partial x^2}.$$

The results that follow are valid if $2\beta<4+\alpha$. In these conditions, we have $\varepsilon\in(0,1/2)$. We denote by $x_F(t)$ the position of the heat front [with $x_F(0)=0$] and by $T_S(t)$ the surface temperature at $x=0$. The heat flux and the temperature vanish at the front, meaning that ζ satisfies $\zeta(t,x_F(t))=0$ and $\partial_x\zeta[t,x_F(t)]=0$.

B. Self-similar solutions

We assume that the surface temperature has the power-law profile for $t \geq 0$

$$T_S(t) = T_{S0}\left(\frac{t}{t_S}\right)^k, \tag{3}$$

where k is a fixed exponent and t_S is an arbitrary time that has been included for consistency of units. As we will see in Sec. II F, it is necessary to assume that

$$\frac{-1}{4+\alpha-\beta} < k < \frac{1}{4+\alpha-2\beta}, \tag{4}$$

and also that the parameters of the problem satisfy the condition

$$2-3\mu+k[4(2-\mu+2\lambda)-\alpha(2-3\mu)-\beta(2+3\lambda)] > 0. \tag{5}$$

The special case $k=0$ corresponds to the step function $T_S(t)=T_{S0}$ for $t \geq 0$. This case is compatible with (4) and (5) if $\mu < 2/3$.

We look for a self-similar solution of the form

$$\zeta(t,x) = \zeta_S(t)\hat{\zeta}\left(\frac{x}{x_F(t)}\right), \tag{6}$$

$$\zeta_S(t) = T_{S0}^{4+\alpha}\left(\frac{t}{t_S}\right)^{q_0}, \quad x_F(t) = x_{F0}\left(\frac{t}{t_S}\right)^n \tag{7}$$

with the normalization $\hat{\zeta}(0)=1$ and $q_0=(4+\alpha)k$. Substituting these ansätze into the nonlinear heat equation, we find that the exponent n is given by

$$n = \frac{1+k(4+\alpha-\beta)}{2}. \tag{8}$$

Furthermore, the length x_{F0} is given by

$$x_{F0} = \sqrt{\Gamma C t_S T_{S0}^{4+\alpha-\beta}}, \tag{9}$$

where Γ is a dimensionless parameter that parameterizes the ordinary differential equation satisfied by the spatial profile $\hat{\zeta}$:

$$\frac{d^2\hat{\zeta}}{dy^2} = \Gamma\varepsilon\left(q_0\hat{\zeta}^{\varepsilon}(y) - ny\hat{\zeta}^{\varepsilon-1}(y)\frac{d\hat{\zeta}}{dy}\right), \tag{10}$$

for $y \in (0,1)$. Here, $y=x/x_F$. This second-order differential equation is supplemented with three boundary conditions:

$$\hat{\zeta}(0) = 1, \quad \hat{\zeta}(1) = 0, \quad \partial_y\hat{\zeta}(1) = 0. \tag{11}$$

Consequently, the system (10) and (11) admits a unique solution $\hat{\zeta}$ for a unique value of the parameter Γ. Note that

- The pair eigenvalue-eigenfunction $(\Gamma, \hat{\zeta})$ depends only on α, β, and k.
- The solution to the nonlinear diffusion equation is unique with the prescribed boundary conditions. Since the function ζ defined by (6) is a solution, it is therefore the unique solution of the problem.

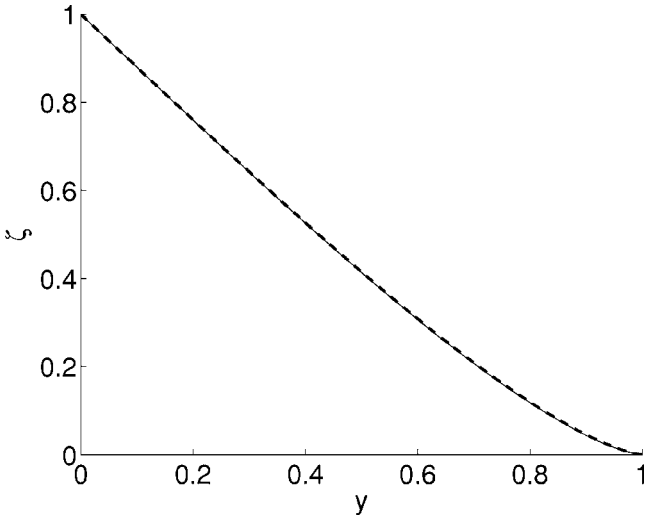

FIG. 1. Spatial profile of the function $\hat{\zeta}$ for the numerical data in (2). The solid line is the profile obtained by the resolution of the nonlinear eigenvalue problem, and the dashed line is the second-order expansion (16). The exact value of Γ is 3.277, while the second-order (third-order) expansion gives $\Gamma=3.155$ ($\Gamma=3.241$).

C. Resolution of the eigenvalue problem

The eigenvalue Γ can be found by a shooting method as follows.

First, we compute the asymptotic expression of the solution $\hat{\zeta}$ near $y=1$. It is easy to check that it has the form

$$\hat{\zeta}(y) = C_a(1-y)^a + o[(1-y)^a]$$

with

$$a = \frac{1}{1-\varepsilon}, \quad C_a = [n\Gamma(1-\varepsilon)]^{1/(1-\varepsilon)}.$$

We then integrate (numerically) backward in space the ordinary differential equation (10) with a terminal condition at $y=1-\delta$, $\delta \ll 1$ (say, $\delta=10^{-10}$):

$$\hat{\zeta}(1-\delta) = C_a\delta^a, \quad \partial_y\hat{\zeta}(1-\delta) = -C_a a\delta^{a-1}.$$

For a given value of Γ, we obtain a value for $\hat{\zeta}(0)$. The shooting method consists of obtaining the value Γ so that $\hat{\zeta}(0)=1$. This can be done by a Newton method that converges exponentially quickly. Indeed, if $\hat{\zeta}(0)<1$, then this means that the tested value Γ is too small, while if $\hat{\zeta}(0)>1$, then this means that the tested value Γ is too large.

Once the algorithm has converged, the obtained value Γ is the eigenvalue of the system (10) and (11), and the function $\hat{\zeta}$ gives the spatial profile of ζ. Substituting the obtained value of Γ into (9), and using (8), we obtain the time evolution of the heat front. In Fig. 1 we plot the spatial profile $y \mapsto \hat{\zeta}(y)$. We use the numerical values (2) and we consider the step function case $k=0$.

D. Flux and energy

The total internal energy is

$$E_i(t) = \int_0^{x_F(t)} \rho e(t,x) dx. \tag{12}$$

Using the relation (1) and the self-similar expression of the temperature profile T, we obtain

$$E_i(t) = f x_{F0} \rho_0^{1-\mu} T_{S0}^{\beta} \left[\int_0^1 \hat{\zeta}^{\varepsilon}(y) dy \right] \left(\frac{t}{t_S} \right)^{n+q_0\varepsilon}.$$

Substituting the expression of x_{F0}, we get

$$E_i(t) = \sqrt{\frac{16}{12+3\alpha}} g f \sigma t_S^{1/2} \rho_0^{-(\mu+\lambda)/2} T_{S0}^{2+(\alpha+\beta)/2} \times \left[\sqrt{\Gamma} \int_0^1 \hat{\zeta}^{\varepsilon}(y) dy \right] \left(\frac{t}{t_S} \right)^{n+q_0\varepsilon}. \tag{13}$$

The value of the square brackets for the numerical data in (2) is 1.318.

The heat flux at the surface is

$$F(t) = -\frac{4}{3} \frac{1}{K\rho} \frac{\partial \sigma T^4}{\partial x} \ (t, x=0). \tag{14}$$

Using the relation (1) and the self-similar expression of the temperature profile T, we obtain

$$F(t) = \frac{16 \sigma g T_{S0}^{4+\alpha}}{(12+3\alpha)\rho_0^{1+\lambda} x_{F0}} \left[-\frac{d\hat{\zeta}}{dy}(y=0) \right] \left(\frac{t}{t_S} \right)^{q_0-n}.$$

Integrating the ordinary differential equation (10) between 0 and 1, we get the identity

$$-\frac{d\hat{\zeta}}{dy}(y=0) = \Gamma(n+q_0\varepsilon) \int_0^1 \hat{\zeta}^{\varepsilon}(y) dy.$$

Using this identity and the expression of x_{F0}, we can check the energy conservation relation $F = \partial_t E_i$.

E. Expansion for $\varepsilon \ll 1$

The shooting method allows us to obtain exact expressions, whatever the value of ε. Note that it is not possible to obtain closed form formulas for the eigenvalue Γ or for the spatial profile $\hat{\zeta}$, but the numerical resolution (a second-order differential equation) is straightforward. However, if ones wishes to obtain analytic expressions, it is possible to expand Γ and $\hat{\zeta}$ in powers of ε. We give here the method in the case $k=0$ (constant surface temperature). Let us consider the auxiliary function $\hat{\psi}(y) = \hat{\zeta}^{1-\varepsilon}(y)$, which satisfies

$$\hat{\psi} \frac{d^2\hat{\psi}}{dy^2} + \frac{\varepsilon\Gamma}{2} y \frac{d\hat{\psi}}{dy} + \frac{\varepsilon}{1-\varepsilon} \left(\frac{d\hat{\psi}}{dy} \right)^2 = 0$$

for $y \in (0,1)$, with the boundary conditions $\hat{\psi}(0)=1$, $\hat{\psi}(1)=0$, and $\partial_y \hat{\psi}(1) = (\varepsilon-1)\Gamma/2$. We can then expand:

$$\Gamma = \sum_{j=0}^{\infty} \Gamma_j \varepsilon^j, \quad \hat{\psi}(y) = (1-y) \sum_{j=0}^{\infty} \varepsilon^j \hat{\psi}_j(y),$$

where $\hat{\psi}_j$ is a polynomial of degree j. By identifying the first corrective terms, we get

$$\Gamma = 2 + 3\varepsilon + \frac{10}{3}\varepsilon^2 + \frac{251}{72}\varepsilon^3 + O(\varepsilon^4), \tag{15}$$

$$\hat{\psi}(y) = (1-y) \left(1 + \varepsilon \frac{y}{2} + \varepsilon^2 \frac{y(1+y)}{12} + \varepsilon^3 \frac{y(1-y)(-3-y-y^2/3)}{48} + O(\varepsilon^4) \right). \tag{16}$$

The comparisons between the expansions and the real values of Γ and $\hat{\zeta}(y) = \hat{\psi}^{1/(1-\varepsilon)}(y)$ are given in Fig. 1. The expansions (15) and (16) are consistent with the ones obtained in Ref. 11, that are valid up to order $O(\varepsilon^3)$.

F. Limit of validity

The supersonic regime is valid as long as the mass set into hydrodynamic motion is smaller than the ablated mass, which means that the heat front located at $x_F(t)$ is ahead of the point $x_H(t)$ moving with the speed of sound. It is also necessary that the velocity of the heat front be larger than the sound velocity, since a shock will be created at this hydrodynamic separation time t_{HS}. The second condition is obviously stronger than the first one.

Let us consider the *general case* $k \in \mathbb{R}$. The isothermal speed of sound is $c = \sqrt{(1-\mu)P/\rho_0}$, where $P(t) = r f T_S^{\beta}(t) \rho_0^{1-\mu}$, and it behaves as $c(t) \sim t^{\beta k/2}$. The front position x_F is given by (7), $x_F(t) \sim t^n$, and its velocity behaves as $\partial_t x_F(t) \sim t^{n-1}$. It is therefore necessary to impose that $n>0$ and $n-1 < k\beta/2$ to ensure that the supersonic regime is valid, which gives the condition (4). The supersonic regime is valid till the hydrodynamic separation time t_{HS} defined by $\partial_t x_F(t_{\mathrm{HS}}) = c(t_{\mathrm{HS}})$. We obtain the explicit expression

$$\frac{t_{\mathrm{HS}}}{t_S} = \left[\frac{4\Gamma g \sigma [1+k(4+\alpha-\beta)]^2}{(12+3\alpha) r (1-\mu) f^2 t_S} \frac{T_{S0}^{4+\alpha-2\beta}}{\rho_0^{2-2\mu+\lambda}} \right]^{1/[1-k(4+\alpha-2\beta)]}. \tag{17}$$

The results derived in this section are valid only in the diffusion-approximation regime. For the diffusion approximation to be valid, the mean free path defined by $l_R := 1/(K\rho)$ should be smaller than the typical temperature gradient length defined by $l_T := (\partial_x T/T)^{-1}$. Here we have

$$l_R(t) \sim g T_S^{\alpha}(t) \rho_0^{-1-\lambda}, \quad l_T(t) \sim x_F(t),$$

so the diffusion approximation regime holds true if

$$x_F(t) \gg g T_S^{\alpha}(t) \rho_0^{-1-\lambda}.$$

This imposes that $t \gg t_{\mathrm{DA}}$, where

$$\frac{t_{\mathrm{DA}}}{t_S}=\left[\frac{gfT_{S0}^{-4+\alpha+\beta}\rho_0^{-\mu-\lambda}}{\sigma t_S}\right]^{1/[1+k(4-\alpha-\beta)]}. \tag{18}$$

To summarize, the supersonic regime is valid during the time interval $t_{\mathrm{DA}}\ll t<t_{\mathrm{HS}}$. The existence of this regime requires that $t_{\mathrm{DA}}\ll t_{\mathrm{HS}}$. This imposes that the condition (5) should be fulfilled: $\xi(k)>0$ with

$$\xi(k)=2-3\mu+k[4(2-\mu+2\lambda)-\alpha(2-3\mu)-\beta(2+3\lambda)],$$

and that the density should be small enough so that $\rho_0\ll\rho_{\mathrm{super}}$, with

$$\rho_{super}=(\sigma T_{S0}^4)^{2/\xi(k)}(fT_{S0}^{\beta})^{-3/\xi(k)}.$$

Let us discuss *the particular case* $k=0$. The isothermal speed of sound is $c_0=\sqrt{(1-\mu)P_0/\rho_0}$, where $P_0=rfT_{S0}^{\beta}\rho_0^{1-\mu}$. The front position x_F is given by (7), its velocity decays as $t^{-1/2}$, while the sound velocity is constant:

$$c_0=\sqrt{fr(1-\mu)}T_{S0}^{\beta/2}\rho_0^{-\mu/2}.$$

Thus, the supersonic condition $\partial_t x_F(t)>c_0$ is satisfied until the critical time t_{HS} given by

$$t_{\mathrm{HS}}=\frac{4\Gamma g\sigma}{(12+3\alpha)r(1-\mu)f^2}T_{S0}^{4+\alpha-2\beta}\rho_0^{-2+2\mu-\lambda}. \tag{19}$$

The results derived in this section are valid only in the diffusion-approximation regime, which imposes that $t\gg t_{\mathrm{DA}}$, where

$$t_{\mathrm{DA}}=\frac{gfT_{S0}^{-4+\alpha+\beta}\rho_0^{-\mu-\lambda}}{\sigma}. \tag{20}$$

To summarize, the results of this section hold true if

$$t_{\mathrm{DA}}\ll t<t_{\mathrm{HS}}. \tag{21}$$

The supersonic regime is valid during this time interval. Note that the existence of this regime requires that $t_{\mathrm{DA}}\ll t_{\mathrm{HS}}$, that is to say $\mu<2/3$, and the density should be small enough so that $\rho_0\ll\rho_{\mathrm{super}}$, where

$$\rho_{\mathrm{super}}=(\sigma T_{S0}^4)^{2/(2-3\mu)}(fT_{S0}^{\beta})^{-3/(2-3\mu)}. \tag{22}$$

In other words, for a fixed time t, the results of this section are valid if the density satisfies

$$\rho_{\mathrm{DA}}(t)\ll\rho_0<\rho_{\mathrm{HS}}(t), \tag{23}$$

where

$$\rho_{\mathrm{HS}}(t)=\left[\frac{4\Gamma g\sigma}{(12+3\alpha)r(1-\mu)f^2t}\right]^{1/(2-2\mu+\lambda)}\times T_{S0}^{(4-2\beta+\alpha)/(2-2\mu+\lambda)}, \tag{24}$$

$$\rho_{\mathrm{DA}}(t)=\left[\frac{gf}{\sigma t}\right]^{1/(\mu+\lambda)}T_{S0}^{(4-\alpha-\beta)/(\mu+\lambda)}. \tag{25}$$

We use the fit to the opacity and equation of state for gold in the temperature range 100–200 eV given in Ref. 12: α, β, μ, λ, and r are given by (2), $f=3.4$ MJ/g, $g=1/7200$ g/cm^2, and $\sigma=1.03\times10^{-2}$ MJ/ns/cm^2, assuming that the temperature is expressed in heV (1 heV =100 eV), the density in g/cm^3, and the time in ns. For $T_{S0}=100$ eV and $t=2$ ns, one finds $\rho_{\mathrm{DA}}\simeq2\times10^{-5}$ g/cm^3 and $\rho_{\mathrm{HS}}=0.14$ g/cm^3. For $T_{S0}=200$ eV and $t=2$ ns, one finds $\rho_{\mathrm{DA}}\simeq3\times10^{-6}$ g/cm^3 and $\rho_{\mathrm{HS}}=0.32$ g/cm^3.

G. The rarefaction wave

We have used in the previous analysis the energy conservation equation and neglected the hydrodynamic motion. A more careful analysis should take into account the hydrodynamic motion described by the mass and momentum conservation equations

$$\frac{\partial\rho}{\partial t}+u\frac{\partial\rho}{\partial x}+\rho\frac{\partial u}{\partial x}=0,$$

$$\frac{\partial u}{\partial t}+u\frac{\partial u}{\partial x}+\frac{1}{\rho}\frac{\partial p}{\partial x}=0.$$

In this section, we assume $k=0$. At time $t=0$, the heat wave penetrates the medium $x>0$. At time $t=0^+$, the fluid around $x=0$ is divided into two regions:

- For $x>0$ the density is ρ_0 and the pressure is $P_0=rf\rho_0^{1-\mu}T_{S0}^{\beta}$.
- For $x<0$, the density and pressure are evanescent.

As a result, a hydrodynamic motion is initiated in the form of an isothermal rarefaction wave. The material expands into the vacuum region, but its temperature is constant. Indeed, the temperature decay is compensated for by the internal energy deposited by the heat flux. The hydrodynamic profiles of the rarefaction wave is a function of x/t only. This can be justified *a priori* by pointing out that no combination of physical parameters has the dimension of space or time. This can also be checked *a posteriori* in the sense that we obtained a solution that is a function of x/t only, which is the solution of the problem because the solution is unique. By self-similarity, the velocity and density profiles are of the form $\rho(t,x)=\hat{\rho}(x/t)$, $u(t,x)=\hat{u}(x/t)$. With the isothermal hypothesis, the pressure is $p(t,x)=rfT_{S0}^{\beta}\rho^{1-\mu}(t,x)$. Substituting into the mass and momentum conservation equations, we obtain the system of ordinary differential equations:

$$(\hat{u}-y)\frac{d\hat{\rho}}{dy}+\hat{\rho}\frac{d\hat{u}}{dy}=0,$$

$$(\hat{u}-y)\frac{d\hat{u}}{dy}+r(1-\mu)fT_{S0}^{\beta}\hat{\rho}^{-1-\mu}\frac{d\hat{\rho}}{dy}=0.$$

This system can be solved analytically if $\mu\in(0,1)$. We find that the rarefaction wave at time t has a spatial extension that goes from $-\infty$ to c_0t, where c_0 is the isothermal speed of sound:

$$c_0^2=\left.\frac{\partial P}{\partial\rho}\right|_{T_{S0}}=r(1-\mu)fT_{S0}^{\beta}\rho_0^{-\mu}.$$

The profiles of the hydrodynamic variables (density and velocity) are

$$\rho(t,x)=\rho_0\left[1+\frac{\mu}{2-\mu}\left(1-\frac{x}{c_0t}\right)\right]^{-2/\mu},$$

$$u(t,x)=\frac{2c_0}{2-\mu}\left(\frac{x}{c_0t}-1\right).$$

Note that, if $\mu=0$, then ρ takes the classical exponential profile (Ref. 13, Sec. 99). The kinetic and internal energies of the material put into hydrodynamic motion are

$$E_c=\frac{1}{2}\int_{-\infty}^{c_0t}\rho(t,x)u(t,x)^2dx=\frac{1}{(1-\mu)(1-3\mu/2)}\rho_0c_0^3t,$$

$$E_i=\frac{1}{r}\int_{-\infty}^{c_0t}p(t,x)dx=\frac{1-\mu/2}{r(1-\mu)(1-3\mu/2)}\rho_0c_0^3t.$$

Thus, the total energy of the fluid put into hydrodynamic motion is

$$E=E_c+E_i=\frac{1+r-\mu/2}{(1-3\mu/2)}\frac{\rho_0c_0^3t}{r(1-\mu)}. \tag{26}$$

On the other hand, without hydrodynamic motion, this fluid in the supersonic phase would have the (internal) energy

$$E_l=\frac{1}{r}\int_0^{c_0t}P_0dx=\frac{\rho_0c_0^3t}{r(1-\mu)}.$$

This shows that, with respect to the supersonic regime, the hydrodynamic motion increases the energy of the region $[0,c_0t]$ by the additional fraction

$$K_c=\frac{1+r-\mu/2}{1-3\mu/2}-1=\frac{r+\mu}{1-3\mu/2}.$$

For the numerical data in (2), we have $K_c=0.49$.

H. Correction to the energy due to the hydrodynamic motion

We still consider the case $k=0$. The energy in the early time steps grows as $\sqrt{t}$ and it is given by (13). The hydrodynamic motion modifies this picture and induces a new term. This term is an increase of the energy of the region $[0,x_H(t)]$ by the factor K_c, where $x_H(t)=c_0t$. As a result, the total energy is

$$E=\sqrt{\Gamma}\left[\int_0^1\hat{\zeta}^{\varepsilon}(y)dy+K_c\int_0^{x_H/x_F(t)}\hat{\zeta}^{\varepsilon}(y)dy\right]\times\sqrt{\frac{16}{12+3\alpha}}\sqrt{gf\sigma}T_{S0}^{2+(\alpha+\beta)/2}\rho_0^{-(\mu+\lambda)/2}t^{1/2},$$

$$\frac{x_H(t)}{x_F(t)}=\sqrt{\frac{(12+3\alpha)r(1-\mu)f^2}{16\Gamma g\sigma}}T_{S0}^{2+\beta-\alpha/2}\rho_0^{1-\mu+\lambda/2}t^{1/2}.$$

By differentiating the expression of the energy with respect to ρ_0, we find that the minimal energy is reached when x_H/x_F is equal to $Q\in(0,1)$, where Q is the first point satisfying

$$\frac{K_cQ\hat{\zeta}^{\varepsilon}(Q)}{\int_0^1\hat{\zeta}^{\varepsilon}(y)dy+K_c\int_0^Q\hat{\zeta}^{\varepsilon}(y)dy}=\frac{\mu+\lambda}{2-2\mu+\lambda}.$$

For the numerical data in (2), we have $Q=0.39$. This corresponds to a density equal to

$$\rho_{\min}=\left[\frac{16\Gamma g\sigma Q^2}{(12+3\alpha)r(1-\mu)f^2}\right]^{1/(2-2\mu+\lambda)}\times t^{-1/(2-2\mu+\lambda)}T_{S0}^{(4-2\beta+\alpha)/(2-2\mu+\lambda)}. \tag{27}$$

Note that $\rho_{\min}$ belongs to the range of validity (23). For instance, using the fit to the opacity and equation of state for gold in the temperature range 100–200 eV given in Ref. 12, one finds $\rho_{\min}=0.11$ g/cm^3 for $T_{S0}=100$ eV and $t=2$ ns, and $\rho_{\min}=0.25$ g/cm^3 for $T_{S0}=200$ eV and $t=2$ ns. It is worth remarking that these values are within 10% of those derived in Ref. 12, which used an approach simpler than the more rigorous and general derivation that we have presented here.

The minimal energy achieved with the optimal density is

$$E_{\min}=C_{\min}[g\sigma T_{S0}^{4+\alpha}]^{(1-3\mu/2)/(2-2\mu+\lambda)}\times[fT_{S0}^{\beta}]^{(1+3\lambda/2)/(2-2\mu+\lambda)}t^{(1-\mu/2+\lambda)/(2-2\mu+\lambda)}, \tag{28}$$

with

$$C_{\min}=\left[\frac{16\Gamma}{12+3\alpha}\right]^{(1-3\mu/2)/(2-2\mu+\lambda)}\times\left[\frac{r(1-\mu)}{Q^2}\right]^{(1/2)(\mu+\lambda)/(2-2\mu+\lambda)}\times\left[\int_0^1\hat{\zeta}^{\varepsilon}(y)dy+K_c\int_0^Q\hat{\zeta}^{\varepsilon}(y)dy\right].$$

For the numerical data in (2), we have $C_{\min}=1.52$. Note that $C_{\min}$ depends only on α, β, μ, λ, and r.

III. SUBSONIC WAVES

A. The model

When taking into account the radiative and hydrodynamic phenomena, the equations in Lagrangian form are

$$\frac{\partial V}{\partial t}=\frac{\partial u}{\partial m},$$

$$\frac{\partial u}{\partial t}=-\frac{\partial P}{\partial m},$$

$$\frac{\partial e}{\partial t}+P\frac{\partial V}{\partial t}=\frac{4}{3}\frac{\partial}{\partial m}\frac{1}{K}\frac{\partial\sigma T^4}{\partial m},$$

where $V=1/\rho$ is the specific volume, u the flow velocity, and $m=\int\rho dx$ the mass variable. In this section, we assume that the initial density ρ_0 of the material is very large, in the sense that it is much larger than the typical density of the ablated material. The forthcoming analysis gives the density profile of the ablated material, so this assumption can be easily checked a posteriori (see Sec. III G).

We denote by $m_F(t)$ the mass coordinate at the heat front and we introduce the new coordinate $y=m/m_F$. The boundary conditions read

$$T(t,0)=T_S(t), \quad \lim_{y\to 0} V(t,y)=\infty, \tag{29}$$

$$u(t,1)=0, \quad V(t,1)=0, \quad T(t,1)=0, \tag{30}$$

which means that the density is evanescent (infinite) at the surface $y=0$ (at the heat front, $y=1$).

B. Self-similar solutions

We assume that the imposed temperature at $y=0$ has the form (3). We look for self-similar solutions of the form

$$T(t,y)=T_S(t)\hat{T}(y), \quad m_F(t)=m_{F0}\left(\frac{t}{t_S}\right)^n, \tag{31}$$

$$V(t,y)=V_S(t)\hat{V}(y), \quad u(t,y)=u_S(t)\hat{u}(y), \tag{32}$$

$$V_S(t)=V_{S0}\left(\frac{t}{t_S}\right)^l, \quad u_S(t)=u_{S0}\left(\frac{t}{t_S}\right)^j, \tag{33}$$

where $\hat{T}(y=0)=1$ in order to satisfy the boundary condition. Substituting these ansätze into the system of partial differential equations, we first identify the exponents n, l, and j:

$$n=\frac{1+\lambda-\frac{3\mu}{2}+\left[1-\frac{\mu}{2}-\varepsilon\left(1-\frac{\lambda}{2}\right)\right]q_0}{2+\lambda-2\mu},$$

$$l=\frac{1-(1-2\varepsilon)q_0}{2+\lambda-2\mu},$$

$$j=n+l-1=\frac{\frac{\mu}{2}+\left[\varepsilon\left(1+\frac{\lambda}{2}\right)-\frac{\mu}{2}\right]q_0}{2+\lambda-2\mu},$$

where $q_0=(4+\alpha)k$ and $\varepsilon=\beta/(4+\alpha)$. These expressions for n, l, and j are precisely the same as Eq. (79) of Ref. 11. In this section, we require that $\mu<1$, $4+\alpha>2\beta$, and that the exponent k satisfies the conditions (5) and

$$\frac{-1-\lambda+3\mu/2}{(4+\alpha)(1-\mu/2)-\beta(1-\lambda/2)}<k<\frac{1}{4+\alpha-2\beta}, \tag{34}$$

in order to ensure the existence and uniqueness of the self-similar solution (see Sec. III G). Note also that these conditions ensure in particular that $\varepsilon\in(0,1/2)$, $n>0$, and $l>0$. The special case $k=0$ corresponds to the step function $T_S(t)=T_{S0}$ for $t\geq 0$. This case is compatible with (34) and (5) if $\mu<2/3$.

By collecting the terms with the same power in t, we find that the quantities V_{S0}, u_{S0}, m_{F0} are of the form

$$m_{F0}=\left(\frac{16}{12+3\alpha}\frac{g\sigma T_{S0}^{4+\alpha}}{\Gamma}\right)^{(1-\mu/2)/(2-2\mu+\lambda)} \times(fT_{S0}^{\beta})^{(-1+\lambda/2)/(2-2\mu+\lambda)} r^{(1/2)(\lambda-\mu)/(2-2\mu+\lambda)} \times t_S^{(1/2)(2-3\mu+2\lambda)/(2-2\mu+\lambda)}, \tag{35}$$

$$V_{S0}=\left(\frac{16}{12+3\alpha}\frac{g\sigma T_{S0}^{4+\alpha-2\beta}}{rf^2\Gamma t_S}\right)^{-1/(2-2\mu+\lambda)}, \tag{36}$$

$$u_{S0}=\frac{m_{F0}V_{S0}}{t_S}, \tag{37}$$

where the parameter Γ appears in the system of ordinary differential equations satisfied by the normalized spatial profiles $\hat{\zeta}=\hat{T}^{4+\alpha}$, $\hat{V}$, $\hat{u}$:

$$\frac{d\hat{V}}{dy}=\frac{nly\hat{V}-\varepsilon\hat{\zeta}^{\varepsilon-1}\hat{V}^{\mu-1}\hat{\xi}-j\hat{u}}{n^2y^2+(\mu-1)\hat{V}^{\mu-2}\hat{\zeta}^{\varepsilon}}, \tag{38}$$

$$\frac{d\hat{u}}{dy}=l\hat{V}-ny\frac{d\hat{V}}{dy}, \tag{39}$$

$$\frac{d\hat{\zeta}}{dy}=\hat{\xi}, \tag{40}$$

$$\frac{d\hat{\xi}}{dy}=\frac{\hat{V}^{-\lambda}}{\Gamma}\left\{[q_0\varepsilon+(\mu+r)l]\hat{\zeta}^{\varepsilon}\hat{V}^{\mu}-\varepsilon ny\hat{\zeta}^{\varepsilon-1}\hat{V}^{\mu}\hat{\xi} -[\lambda\Gamma\hat{V}^{\lambda-1}\hat{\xi}+ny(\mu+r)\hat{\zeta}^{\varepsilon}\hat{V}^{\mu-1}]\frac{d\hat{V}}{dy}\right\}. \tag{41}$$

This system (38)–(41) consists of four first-order ordinary differential equations; it possesses one free parameter Γ, and it is complemented with the five boundary conditions (29) and (30). As a result, the value of the parameter Γ can be fixed, and the existence and expressions of the spatial profiles of the self-similar solution can be obtained. We deal with a well-posed problem. In contrast to previous work,[11,12] perturbation expansions are not needed.

The idea to find the eigenvalue Γ and the eigenfunctions $(\hat{\zeta},\hat{V},\hat{u})$ is to use a shooting method. This method was used by Pakula and Siegel in a similar situation in the case $\mu=0$.[8] In our paper, the μ dependence is very important because it plays a critical role in the density dependence of the energy lost by ablating the wall. The ideal shooting method would consist in solving the system (38)–(40) with four initial conditions and an arbitrary parameter Γ, and to make the parameter Γ converge to the value that ensures that the complete set of boundary conditions (29) and (30) is satisfied. Unfortunately, the five boundary conditions are split in a group of three at $y=1$, and a group of two at $y=0$. It is therefore necessary to apply a shooting method at two dimensions; the parameter Γ and an additional boundary condition at $y=1$ will be matched to ensure that the two boundary conditions (29) are satisfied. We give more detail below, but before we need *a priori* estimates on the behavior of the solution at the boundary $y=1$.

C. Expansions of the solution close to $y=1$

The solutions can be expanded at $y=1$ as

$$\hat{\zeta}(y) = C_a(1-y)^a + o[(1-y)^a],$$

$$\hat{V}(y) = C_b(1-y)^b + o[(1-y)^b],$$

$$\hat{u}(y) = C_c(1-y)^c + o[(1-y)^c],$$

with

$$a = \frac{1-\mu}{1-\varepsilon-\mu+\varepsilon\lambda}, \quad c = b = \frac{\varepsilon}{1-\varepsilon-\mu+\varepsilon\lambda},$$

$$C_a = \left(\frac{n(b\mu+a\varepsilon)+brn}{\Gamma a(b\lambda+a-1)}\right)^{1/(1-\varepsilon)} C_b^{(\mu-\lambda)/(1-\varepsilon)}, \quad C_c = -nC_b,$$

while $C_b > 0$ is free.

D. Shooting method

We describe in this subsection the shooting method. We consider an evanescent point δ_0 (say, $\delta_0 = 10^{-10}$).

(1) We consider a value for the parameter Γ. We perform a Newton algorithm to determine the parameter C_b as follows.

(a) We consider a value for the parameter $C_b > 0$.
(b) We solve backward in space the system (38)–(41) from $y = 1-\delta_0$ with the terminal conditions

$$\zeta_0 = C_a\delta_0^a, \quad V_0 = C_b\delta_0^b, \quad u_0 = C_c\delta_0^c, \quad \xi_0 = -aC_a\delta_0^{a-1}.$$

(c) If $\hat{V}(y)$ has not blown up before $y=0$ (that is to say, between 0 and 1), then we increase C_b. If $\hat{V}(y)$ has blown up before $y=0$, then we decrease C_b. We go back to (a).

(2) This algorithm converges exponentially quickly to the value C_b^Γ, for which $\hat{V}$ blows up just at $y=0$. For this value, the function $\hat{\zeta}(y)$ has a limit $\hat{\zeta}^\Gamma$ as $y \to 0$. This algorithm is actually one step of the super-algorithm that determines the eigenvalue Γ. This super-algorithm proceeds as follows: If the limit $\hat{\zeta}^\Gamma$ is larger than 1, then we come back to (1) with a larger value of Γ. If the limit $\hat{\zeta}^\Gamma$ is smaller than 1, then we come back to (1) with a smaller value of Γ. The super-algorithm converges exponentially fast to the pair of values $(\Gamma, \hat{\zeta}^\Gamma = 1)$, which are such that $\hat{V}(y)$ blows up as $y \to 0$ and $\hat{\zeta}(0) = 1$. This value of Γ is the one that we are looking at, and we also obtain the spatial profiles $\hat{V}$, $\hat{u}$, and $\hat{\zeta}$.

We plot in Fig. 2 the spatial profiles of the hydrodynamic variables for the numerical data in (2), and we give in the next subsection the evolutions of physically relevant quantities.

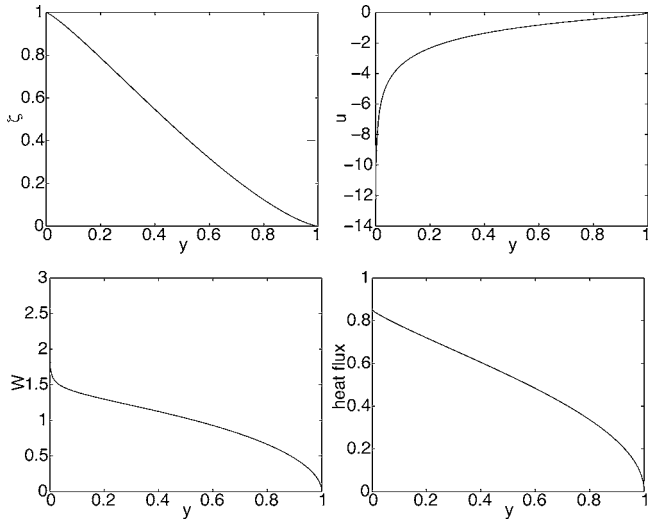

FIG. 2. Spatial profiles (in Lagrangian coordinates $y = m/m_F$) of the functions $\hat{\zeta}(y)$, $\hat{u}(y)$, $\hat{W}(y) = y\hat{V}(y)$, and the normalized heat flux $-\Gamma\hat{V}^\lambda(y)\partial_y\hat{\zeta}(y)$, for the numerical data in (2). The value of Γ is 0.4199.

E. Subsonic results

The heat flux through the surface defined by (14) is

$$F(t) = F_{S0}\left(\frac{t}{t_S}\right)^{n+2j-1}$$

with

$$F_{S0} = \frac{m_{F0}}{t_S} f V_{S0}^\mu T_{S0}^\beta \left[-\Gamma \lim_{y\to 0} \hat{V}^\lambda(y)\partial_y\hat{\zeta}(y)\right].$$

For the numerical data in (2), and $k=0$, the value of the constant term between the square brackets is 0.85.

The total energy is

$$E(t) = \int_0^{m_F(t)} e(t,m) + \frac{1}{2}u^2(t,m)dm = m_{F0} f V_{S0}^\mu T_{S0}^\beta \mathcal{E}_c \left(\frac{t}{t_S}\right)^{n+2j}, \tag{42}$$

where

$$\mathcal{E}_c = \int_0^1 \hat{\zeta}^\varepsilon(y)\hat{V}^\mu(y) + \frac{r}{2}\hat{u}^2(y)dy.$$

For the numerical data in (2), and $k=0$, we have $\mathcal{E}_c \simeq 1.45$. The energy conservation is satisfied, in the sense that $\partial_t E = F$ because

$$-\Gamma \lim_{y\to 0} \hat{V}^\lambda(y)\partial_y\hat{\zeta}(y) = (n+2j)\mathcal{E}_c.$$

The explicit expression of the constant term that appears in (42) is

$$m_{F0} f V_{S0}^\mu T_{S0}^\beta = \left[\frac{16g\sigma T_{S0}^{4+\alpha}}{(12+3\alpha)\Gamma}\right]^{(1-3\mu/2)/(2-2\mu+\lambda)} \times \left[f T_{S0}^\beta\right]^{(1+3\lambda/2)/(2-2\mu+\lambda)} r^{(1/2)(\mu+\lambda)/(2-2\mu+\lambda)} \times t_S^{(1-\mu/2+\lambda)/(2-2\mu+\lambda)}.$$

As a result, if $k=0$, then the complete expression of the energy in the subsonic regime is

$$E_{\mathrm{sub}} = C_{\mathrm{sub}}[g\sigma T_{S0}^{4+\alpha}]^{(1-3\mu/2)/(2-2\mu+\lambda)} \times [fT_{S0}^{\beta}]^{(1+3\lambda/2)/(2-2\mu+\lambda)} t^{(1-\mu/2+\lambda)/(2-2\mu+\lambda)}, \tag{43}$$

where

$$C_{\mathrm{sub}} = r^{(1/2)(\mu+\lambda)/(2-2\mu+\lambda)} \left[\frac{16}{(12+3\alpha)\Gamma}\right]^{(1-3\mu/2)/(2-2\mu+\lambda)} \mathcal{E}_c.$$

For the numerical data in (2) corresponding to gold, and $k=0$, we have $C_{\mathrm{sub}}=1.82$. Note that C_{sub} depends only on α, β, μ, λ, and r. By comparing with (28), we can see that the minimal energy $E_{\min}$ that can be obtained with an optimized low-density material is smaller than the energy obtained with a high-density material by a factor $\sim 17\%$. This optimal gain factor is independent of the temperature T_{S0} or time t, but the optimal density for which this gain is achieved depends on T_{S0} and t. These results are in agreement with the ones obtained by Rosen and Hammer[12] with a perturbation theory.

The ablation pressure (at the heat front) is

$$P(t) = rfT_{S0}^{\beta} V_{S0}^{\mu-1} \left[\lim_{y\to 1} \hat{\xi}^{\varepsilon}(y)\hat{V}^{\mu-1}(y)\right] \left(\frac{t}{t_S}\right)^{2j-l}. \tag{44}$$

For the numerical data in (2), and $k=0$, the value of the constant term between the square brackets is 0.84. The explicit expression of the constant term that appears in (44) is

$$rfT_{S0}^{\beta} V_{S0}^{\mu-1} = \left[\frac{16g\sigma T_{S0}^{4+\alpha}}{(12+3\alpha)\Gamma}\right]^{(\mu-1)/(2-2\mu+\lambda)} \times [fT_{S0}^{\beta}]^{(\lambda/(2-2\mu+\lambda)} r^{(1-\mu+\lambda)/(2-2\mu+\lambda)} t_S^{(1-\mu)/(2-2\mu+\lambda)}.$$

Finally, the momentum (mass flow) at the heat front is

$$M_F(t) := \lim_{m\to m_F} V^{-1}(t,m)u(t,m) = V_S^{-1}(t)u_S(t)\lim_{y\to 1}\hat{V}^{-1}(y)\hat{u}(y).$$

Using the expansion of the hydrodynamic variables at $y=1$ obtained in Sec. III C, we get

$$M_F(t) = -nV_S^{-1}(t)u_S(t) = -n\frac{m_{F0}}{t_S}\left(\frac{t}{t_S}\right)^{n-1}.$$

F. Self-similar profiles in the real space

We can express the Eulerian coordinate x in terms of the Lagrangian coordinate m, known functions of time t, and the unknown heat front position $x_F(t)$. We have

$$x_F(t) - x(t,m) = \int_m^{m_F(t)} V(t,m')dm' = m_F(t)V_S(t)\int_{m/m_F(t)}^1 \hat{V}(\xi)d\xi.$$

In terms of the time t and the self-similar variable y,

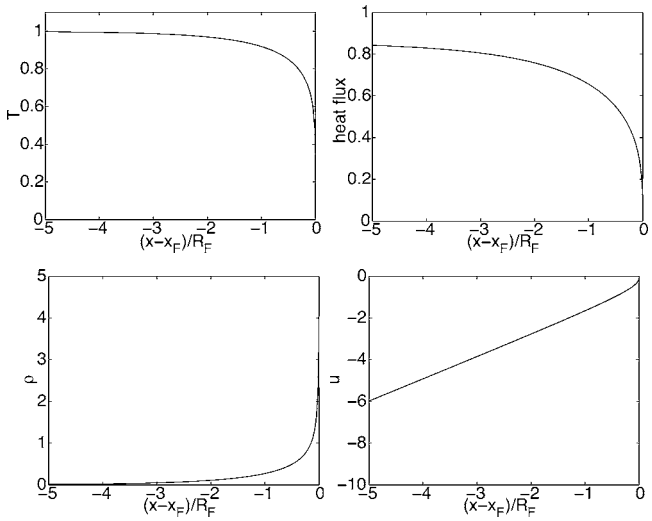

FIG. 3. Spatial profiles (in real space) of the temperature, heat flux, density, and velocity. Here, $R_F(t)=m_F(t)V_S(t)$. We use the numerical data in (2).

$$x(t,y) = x_F(t) - R_F(t)\int_y^1 \hat{V}(\xi)d\xi,$$

where $R_F(t)=m_F(t)V_S(t)$ is the typical thickness of the expanded material. The function $y\mapsto -\int_y^1 \hat{V}(\xi)d\xi$ defined from $(0,1)$ onto $(-\infty,0)$ is continuous and decreasing, so that it can be inverted, which gives the function $\tilde{y}\mapsto\Psi(\tilde{y})$ defined from $(-\infty,0)$ onto $(0,1)$. The inverse function of $y\mapsto x(t,y)$ can then be written as

$$Y_t(x) = \Psi\left(\frac{x-x_F(t)}{R_F(t)}\right).$$

We can then plot the spatial profiles of the hydrodynamic quantities in terms of the Eulerian coordinate x (see Fig. 3). For instance, the temperature profile is

$$T(t,x) = \begin{cases} 0 & \text{if } x \geq x_F(t) \\ T_S(t)\hat{\xi}^{1/(4+\alpha)}[Y_t(x)] & \text{if } x < x_F(t) \end{cases}.$$

G. Limit of validity

The results derived in this section are valid in the diffusion-approximation regime and with the assumption of an infinitely dense initial material.

We first consider the *general case* $k\in\mathbb{R}$. For the diffusion approximation to be valid, the mean free path l_R should be smaller than the typical temperature gradient length l_T, where

$$l_R(t) \sim gT_S^{\alpha}(t)V_S^{1+\lambda}(t), \quad l_T(t) \sim m_F(t)V_S(t),$$

so the diffusion approximation regime holds true if $m_F(t) \gg gT_S^{\alpha}(t)V_S^{\lambda}(t)$. This imposes that $n-\alpha k-\lambda l>0$ [which is equivalent to (5)] and $t \gg t_{\mathrm{DA}}^{(\mathrm{sub})}$, with

$$\frac{t_{\mathrm{DA}}^{(\mathrm{sub})}}{t_S} = \left[\frac{gT_{S0}^{\alpha}V_{S0}^{\lambda}}{m_{F0}}\right]^{1/(n-\alpha k-\lambda l)}.$$

The assumption of an infinitely dense initial material is valid if $\rho_0 \gg V_S^{-1}(t)$, where ρ_0 is the initial material density. This

imposes that $l>0$ [which is equivalent to the second inequality in (34)] and

$$\frac{t}{t_S} \gg [V_{S0}\rho_0]^{-1/l},$$

or else $t \gg t_{\mathrm{HS}}$, where t_{HS} is defined by (17). Finally, the front should start from zero, which imposes $n>0$, which is equivalent to the first inequality in (34).

We now discuss the *particular case* $k=0$. The diffusion approximation is valid if $\mu<2/3$ and $t \gg t_{\mathrm{DA}}^{(\mathrm{sub})}$, where

$$t_{DA}^{(sub)} = (\sigma T_{S0}^4)^{-(1-\mu/2+\lambda)/(1-3\mu/2)} (g T_{S0}^{\alpha})(f T_{S0}^{\beta})^{(1+3\lambda/2)/(1-3\mu/2)}. \tag{45}$$

Note that $t_{\mathrm{DA}}^{(\mathrm{sub})}$ is equal to t_{DA} defined by (20), where we substitute $\rho_{\mathrm{super}}=[(\sigma T_{S0}^4)^{-1}(f T_{S0}^{\beta})^{3/2}]^{-1/(1-3\mu/2)}$ [defined by (22)] for ρ_0.

The assumption of an infinitely dense initial material is valid if $t \gg t_{\mathrm{HS}}$, where t_{HS} is defined by (19).

There exists a last condition for validity: the radiation pressure and energy should be negligible. This condition is fulfilled if $\sigma T^4 \ll cP$, where c is the speed of light, which means

$$\sigma T_S^4(t) \ll rcf T_S^{\beta}(t) V_S^{\mu-1}(t).$$

This imposes that $t \ll t_{\mathrm{rad}}$, where

$$t_{\mathrm{rad}} = (\sigma T_{S0}^4)^{-(1-\mu+\lambda)/(1-\mu)} (g T_{S0}^{\alpha})(f T_{S0}^{\beta})^{\lambda/(1-\mu)} c^{(2-2\mu+\lambda)/(1-\mu)}. \tag{46}$$

In ICF, we usually have $\max(t_{\mathrm{HS}}, t_{\mathrm{DA}}^{(\mathrm{sub})})=t_{\mathrm{HS}}$. As a consequence, the results of this section are valid during the time interval

$$t_{\mathrm{HS}} \ll t \ll t_{\mathrm{rad}}, \tag{47}$$

where t_{HS} and t_{rad} are given by (19) and (46), respectively. The first inequality means that, for a given time t, the initial density ρ_0 should be larger than $\rho_{\mathrm{HS}}(t)$ given by (24).

IV. SELF-SIMILARITY IN THE CRITICAL CASE

In this section we assume that the initial density ρ_0 of the material is arbitrary and that the surface temperature has the power-law profile (3) with the critical exponent

$$k = \frac{1}{4+\alpha-2\beta}.$$

A. Self-similar solution

We denote by $m_F(t)$ the mass coordinate at the heat front and we introduce the new coordinate $y=m/m_F$. The boundary conditions read

$$T(t,0) = T_S(t), \quad \lim_{y\to 0} V(t,y) = \infty, \tag{48}$$

$$u(t,1) = 0, \quad V(t,1) = \frac{1}{\rho_0}, \quad T(t,1) = 0. \tag{49}$$

We look for self-similar solutions of the form (31)–(33) with $V_{S0}=1/\rho_0$, $\hat{T}(y=0)=1$, and $\hat{V}(y=1)=1$ in order to satisfy the boundary conditions (48) and (49). Substituting these ansätze into the system of partial differential equations, we first identify the exponents n, l, and j:

$$n = 1 + \frac{1}{2}\frac{\beta}{4+\alpha-2\beta}, \quad l=0, \quad j=n-1.$$

Note that the choice of the critical exponent for the power-law surface temperature is responsible for the regime $l=0$, which means that the density profile is invariant; i.e., it depends only on the self-similar variable y, and not on time t. As a result, it can satisfy the boundary condition at $y=1$ at all times, and a global self-similar flow is possible as we see below. Here, we require that $\mu<1$ and $4+\alpha>2\beta$ in order to ensure the existence and uniqueness of the self-similar solution. By collecting the terms with the same power in t, we find that the quantities u_{S0} and m_{F0} are given by

$$m_{F0} = r^{1/2} f^{1/2} T_{S0}^{\beta/2} \rho_0^{1-\mu/2} t_S \Gamma, \quad u_{S0} = \frac{m_{F0}}{t_S \rho_0}, \tag{50}$$

where the parameter Γ appears in the system of ordinary differential equations satisfied by the normalized spatial profiles $\hat{\xi}=\hat{T}^{4+\alpha}$, $\hat{V}$, $\hat{u}$:

$$\frac{d\hat{V}}{dy} = \frac{-\varepsilon\hat{\xi}^{\varepsilon-1}\hat{V}^{\mu-1}\hat{\xi} - (n-1)\Gamma^2\hat{u}}{n^2\Gamma^2 y^2 + (\mu-1)\hat{V}^{\mu-2}\hat{\xi}^{\varepsilon}}, \tag{51}$$

$$\frac{d\hat{u}}{dy} = -ny\frac{d\hat{V}}{dy}, \tag{52}$$

$$\frac{d\hat{\xi}}{dy} = \hat{\xi}, \tag{53}$$

$$\frac{d\hat{\xi}}{dy} = \frac{\Gamma^2\hat{V}^{-\lambda}}{\chi_0}\left\{2(n-1)\hat{\xi}^{\varepsilon}\hat{V}^{\mu} - \varepsilon n y \hat{\xi}^{\varepsilon-1}\hat{V}^{\mu}\hat{\xi} - \left[\lambda\frac{\chi_0}{\Gamma^2}\hat{V}^{\lambda-1}\hat{\xi} + ny(\mu+r)\hat{\xi}^{\varepsilon}\hat{V}^{\mu-1}\right]\frac{d\hat{V}}{dy}\right\}. \tag{54}$$

Here, χ_0 is the dimensionless parameter

$$\chi_0 = \frac{16 g \sigma T_{S0}^{4+\alpha-2\beta}}{r f^2 (12+3\alpha)\rho_0^{2-2\mu+\lambda} t_S}, \tag{55}$$

which is an increasing function of the surface temperature parameter T_{S0} (because $4+\alpha>2\beta$) and a decaying function of the initial density ρ_0 (because $\mu<1$). The T_{S0} and ρ_0 dependences of the self-similar profiles and of the eigenvalue Γ are entirely characterized by the parameter χ_0. The system (51)–(54) consists of four first-order ordinary differential equations; it possesses one free parameter Γ, and it is complemented with the five boundary conditions:

$$\lim_{y\to 0}\hat{V}(y) = \infty, \quad \lim_{y\to 0}\hat{\xi}(y) = 1, \tag{56}$$

$$\lim_{y\to 1}\hat{u}(y) = 0, \quad \lim_{y\to 1}\hat{V}(y) = 1, \quad \lim_{y\to 1}\hat{\xi}(y) = 0. \tag{57}$$

B. The isothermal shock

The system (51)–(54) should be solved from $y=1$ to $y=0$. The system presents a pseudo-singularity at $y=1$ because $\hat{\zeta}(1)=0$. However, it is possible to remove this singularity by writing the expansions of the self-similar profiles at $y=1$. We obtain

$$\hat{\zeta}(y) = C_a(1-y)^a + o[(1-y)^a],$$

$$\hat{V}(y) = 1 + C_b(1-y)^b + o[(1-y)^b],$$

$$\hat{u}(y) = C_c(1-y)^c + o[(1-y)^c],$$

with

$$a = \frac{1}{1-\varepsilon}, \quad b = c = \frac{\varepsilon}{1-\varepsilon},$$

$$C_a = \left(\frac{(1-\varepsilon)n\Gamma^2}{\chi_0}\right)^{\frac{1}{1-\varepsilon}}, \quad C_b = -\frac{C_a^{\varepsilon}}{n^2\Gamma^2}, \quad C_c = \frac{C_a^{\varepsilon}}{n\Gamma^2}.$$

The system (51)–(54) is solved from $y=1-\delta_0$ with a very small δ_0 with the terminal conditions

$$\hat{\zeta}_0 = C_a\delta_0^a, \quad \hat{V}_0 = 1 + C_b\delta_0^b,$$
$$\hat{u}_0 = C_c\delta_0^c, \quad \hat{\xi}_0 = -aC_a\delta_0^{a-1}. \tag{58}$$

We should now find the value Γ such that the solution of the system satisfies the two boundary conditions $\lim_{y\to 0}\hat{V}(y)=\infty$ and $\hat{\zeta}(0)=1$ at $y=0$. It seems that it is not possible to satisfy these two additional conditions with a single free parameter. However, the system (51)–(54) exhibits another difficulty as well as an additional degree of freedom, because it presents a singularity: the denominator in Eq. (51) for the density vanishes at some point y_b, and a numerical solver cannot go through this singularity. The only way to go through this singularity is to introduce a shock at some position $y_c > y_b$, which exhibits a density jump. Such a phenomenon has been observed in the study of the structure of a stationary shock wave in Ref. 14, where it was shown that the density presents a discontinuity if the shock is strong enough. Although our configuration is different in that we deal with a self-similar flow, and not a stationary one, it exhibits an isothermal shock, as we see below. This phenomenon has also been pointed out in the pioneering work of Marshak,[1] who considered the same problem in the case $\beta=1$, $\mu=0$. The Rankine Hugoniot relations for the values of the hydrodynamic quantities at the right (y_c^+) and at the left (y_c^-) of the shock position (y_c) can be obtained from the conservation equations for the mass, momentum, and energy, written in conservative forms. They read

$$[\hat{u} + ny_c\hat{V}]_-^+ = 0, \tag{59}$$

$$[\hat{V}^{\mu-1}\hat{\zeta}^{\varepsilon} - \Gamma^2 ny_c\hat{u}]_-^+ = 0, \tag{60}$$

$$[\hat{\zeta}]_-^+ = 0, \tag{61}$$

$$\left[\frac{\chi_0}{\Gamma^2}\hat{\xi}\hat{V}^{\lambda} + ny_c\left(\frac{r\Gamma^2}{2}\hat{u}^2 + \hat{\zeta}^{\varepsilon}\hat{V}^{\mu}\right) - r\hat{\zeta}^{\varepsilon}\hat{V}^{\mu-1}\hat{u}\right]_-^+ = 0. \tag{62}$$

The relation (61) shows that the shock is isothermal, and exhibits a discontinuity only in the density, velocity, and heat flux. Equations (59) and (60) can be combined to obtain the new relation

$$\psi(\hat{V}(y_c^-)) = \psi(\hat{V}(y_c^+)), \tag{63}$$

where $\psi(V) = V^{\mu-1}\hat{\zeta}^{\varepsilon}(y_c) + \Gamma^2 n^2 y_c^2 V$. The function $V \mapsto \psi(V)$ is decaying from 0 to $V_{\min}$, and increasing from $V_{\min}$ to ∞, with

$$V_{\min} = \left(\frac{(1-\mu)\hat{\zeta}^{\varepsilon}(y_c)}{n^2\Gamma^2 y_c^2}\right)^{1/(2-\mu)}.$$

Equation (63) satisfied by the quantity $\hat{V}(y_c^-)$ thus admits a unique solution distinct from $\hat{V}(y_c^+)$. The shock imposes a jump of the density so that $\hat{V}$ jumps from the value $\hat{V}(y_c^+)$, which is smaller than $V_{\min}$ to the value $\hat{V}(y_c^-)$, which is larger than $V_{\min}$. The derivative $\psi'(V)$ also experiences a change of sign. Note that this derivative is the denominator that appears in (51). This shows that the shock allows us to go through the singularity of the system (51)–(54).

We thus have two degrees of freedom: Γ and y_c. For given values of Γ and y_c, the numerical resolution of the system involves three steps:

1. Equations (51)–(54) are integrated from $1-\delta_0$ to y_c^+ with the terminal conditions (58) at $y=1-\delta_0$.
2. The jump conditions (59)–(62) are applied. They can be written explicitly as

$$\hat{\zeta}(y_c^-) = \hat{\zeta}(y_c^+), \quad \psi(\hat{V}(y_c^-)) = \psi(\hat{V}(y_c^+)), \tag{64}$$

$$\hat{u}(y_c^-) = \hat{u}(y_c^+) + ny_c[\hat{V}(y_c^+) - \hat{V}(y_c^-)], \tag{65}$$

$$\hat{\xi}(y_c^-) = \hat{\xi}(y_c^+)\frac{\hat{V}^{\lambda}(y_c^+)}{\hat{V}^{\lambda}(y_c^-)} + \frac{\Gamma^2}{\chi_0\hat{V}^{\lambda}(y_c^-)}\left\{ny_c\frac{r\Gamma^2}{2}[\hat{u}^2(y_c^-) - \hat{u}^2(y_c^+)] + ny_c\hat{\zeta}^{\varepsilon}(y_c)[\hat{V}^{\mu}(y_c^-) - \hat{V}^{\mu}(y_c^+)] - r\hat{\zeta}^{\varepsilon}(y_c) \times [\hat{V}^{\mu-1}\hat{u}(y_c^-) - \hat{V}^{\mu-1}\hat{u}(y_c^+)]\right\}. \tag{66}$$

3. Equations (51)–(54) are integrated from y_c^- to 0 with the terminal conditions (65) and (66) at $y=y_c^-$.

A shooting method allows us to obtain the values of the parameters Γ and y_c that ensure that the solutions satisfy the two boundary conditions $\lim_{y\to 0}\hat{V}(y)=\infty$ and $\hat{\zeta}(0)=1$ at $y=0$. In Figs. 4–6, we plot the density, velocity, and temperature profiles, respectively, obtained with different values of χ_0.

For large values of χ_0 (Fig. 4), that is to say, for small initial density, thermal conduction plays a significant role in the whole region $[0,1]$. The thermal wave presents two distinct parts separated by an isothermal shock at y_c. From the heat front $y=1$ to the isothermal shock y_c, the thermal wave involves a small increase of the density. This part of the

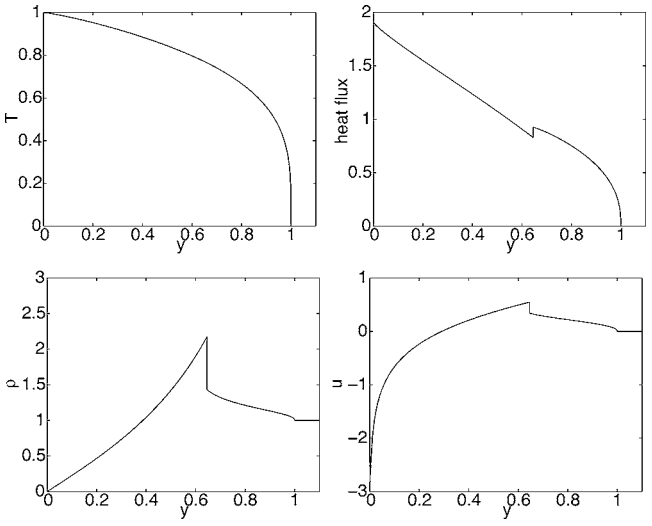

FIG. 4. Spatial profiles of the dimensionless temperature $\hat{T}(y)=\hat{\zeta}^{1/(4+\alpha)}(y)$, heat flux (73), density $\hat{\rho}(y)=1/\hat{V}(y)$, and velocity $\hat{u}(y)$. Here, $\chi_0=2$. The isothermal shock is clearly seen at $y_c\simeq 0.65$.

wave is supersonic, which means that it is not affected by hydrodynamic perturbations coming from the surface conditions at $y=0$. From the isothermal shock y_c to the surface $y=0$, the wave is subsonic.

This structure is general whatever the value of χ_0, but when χ_0 becomes small (see Fig. 5), that is to say, when the initial density becomes large enough, the isothermal shock position y_c becomes very close to the heat front 1. In such a case, as seen in Fig. 5, thermal conduction does not play a significant role in some region $[y_a,1]$, where y_a can be seen as an ablation front. The isothermal shock is actually almost a classical shock. We discuss this case in detail in the next subsection.

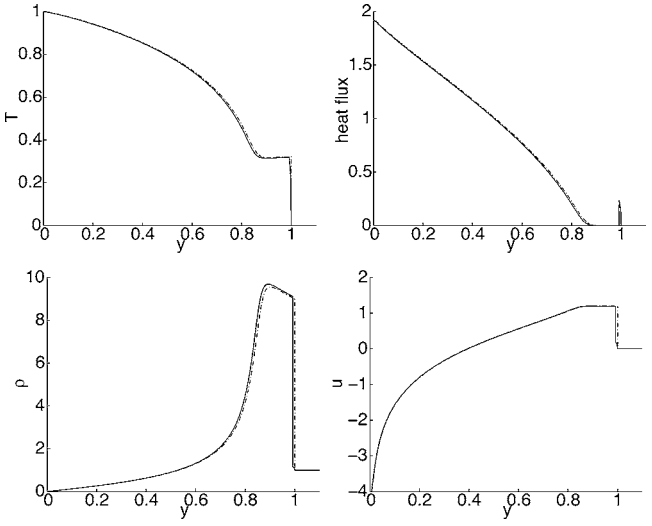

FIG. 5. Spatial profiles of the temperature, heat flux, density, and velocity. Here, $\chi_0=0.45$. The solid lines (dashed lines) stand for the profiles obtained from the numerical integration of the full system (the simplified system). The isothermal shock is very close to the front $y_c\simeq 1$, and it is similar to a classical strong shock. An ablation front appears at $y_a\simeq 0.9$.

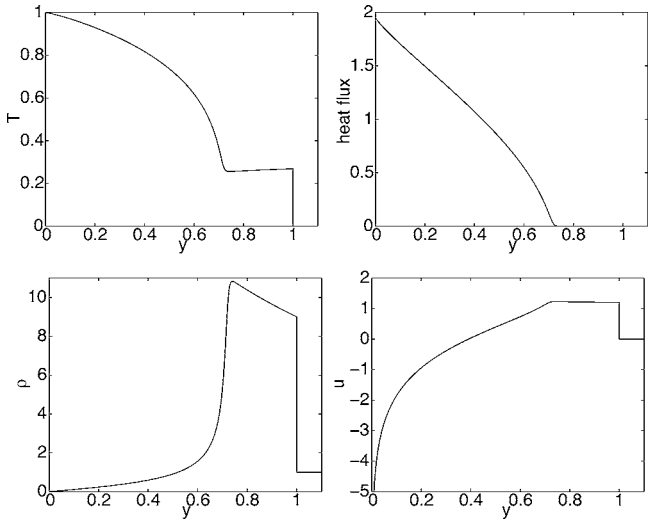

FIG. 6. Spatial profiles of the temperature, heat flux, density, and velocity. Here, $\chi_0=0.25$. The ablation front is noticeable at $y_a\simeq 0.74$.

C. The ablation front

When χ_0 is small, the isothermal shock position y_c becomes very close to $y=1$. It is difficult, from the numerical point of view, to solve the system of ordinary differential equations (51)–(54) that becomes very stiff. We then use the last remark of the previous subsection. We model the isothermal shock as a classical shock in the strong shock approximation regime. Using the boundary conditions $\hat{V}(1^+)=1$, $\hat{u}(1^+)=0$, and $\hat{\zeta}(1^+)=0$, the Rankine Hugoniot relations give the following values:

$$\hat{V}(1^-)=\frac{r}{r+2},\quad \hat{u}(1^-)=\frac{2n}{(r+2)\Gamma}, \tag{67}$$

$$\hat{\zeta}(1^-)=\left(2n^2\frac{r^{1-\mu}}{(2+r)^{2-\mu}}\right)^{1/\varepsilon}. \tag{68}$$

As observed from the numerical integration of the complete system, thermal conduction is negligible in some region $[y_a,1]$. As a consequence, we can consider in this region a simplified version of the system (51)–(54), where thermal conduction is neglected. This system reads

$$\frac{d\hat{V}}{dy}=\frac{-2(n-1)\hat{\zeta}^{\varepsilon}\hat{V}^{\mu-1}-n(n-1)\Gamma^2 y\hat{u}}{ny[n^2\Gamma^2y^2-(1+r)\hat{V}^{\mu-2}\hat{\zeta}^{\varepsilon}]}, \tag{69}$$

$$\frac{d\hat{u}}{dy}=-ny\frac{d\hat{V}}{dy}, \tag{70}$$

$$\frac{d\hat{\zeta}}{dy}=\frac{4n-3}{ny}\hat{\zeta}-\frac{r+\mu}{\varepsilon}\hat{\zeta}\hat{V}^{-1}\frac{d\hat{V}}{dy}. \tag{71}$$

Accordingly, for given values of Γ and y_a, the resolution of the simplified system involves three steps:

1. The strong shock approximation (67) and (68) is applied to get the values of the hydrodynamic quantities at $y=1^-$.

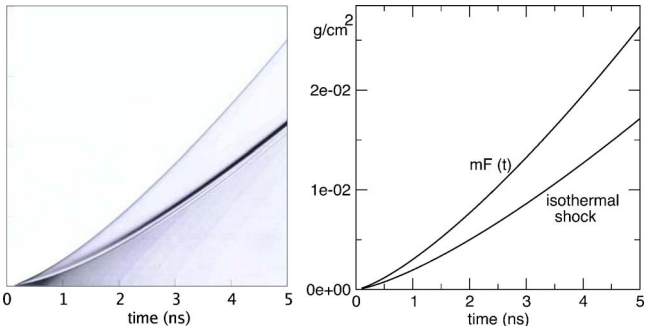

FIG. 7. Time evolution of the temperature front and isothermal shock, obtained with the code (left) and analytic model (right), with $\chi_0=2$.

2. The simplified hydrodynamic system (69)–(71) is integrated from 1^- to y_a.
3. The complete system (51)–(54) is integrated from y_a to 0.

A shooting method allows us to obtain the values of the parameters Γ and y_a that ensure that the solutions satisfy the two boundary conditions $\lim_{y\to 0}\hat{V}(y)=\infty$ and $\hat{\xi}(0)=1$ at $y=0$.

For $\chi_0=0.45$, we can compare the self-similar profiles obtained from the integration of the complete system and the ones obtained from the simplified procedure. This shows that the simplified procedure is very efficient for χ_0 smaller than 0.45. As a result, for smaller values of χ_0, the simplified procedure can be used to get the self-similar profiles of the hydrodynamic quantities. As seen in Fig. 6, where $\chi_0=0.25$, the thermal wave consists of a classical shock at $y=1$, a region $[y_a,1]$ where conduction is negligible, an ablation front at y_a, and an ablative wave in $[0,y_a]$. Remember that the flow is globally self-similar, which means that this structure is generated at time $t=0$. In other words, a shock is emitted at time 0 and it is followed by the ablation front. This structure experiences an expansion described by the function $m_F(t)\sim t^n$ given by (33) and (50).

It is possible to express the self-similar profiles in the physical variables x and t by following the method described in Sec. III F. Here, the real position of the front $y=1$ is $x_F(t)=m_F(t)/\rho_0$ and the thickness is $R_F(t)=x_F(t)$.

The heat flux through the surface defined by (14) is given by

$$F(t)=\tilde{F}(\chi_0)r^{(1/2)(\mu+\lambda)/(2-2\mu+\lambda)}t_s^{(1-\mu/2+\lambda)/(2-2\mu+\lambda)-1}\times\left[\frac{16g\sigma T_{S0}^{4+\alpha}}{12+3\alpha}\right]^{(1-3\mu/2)/(2-2\mu+\lambda)}[fT_{S0}^{\beta}]^{(1+3\lambda/2)/(2-2\mu+\lambda)}\times\left(\frac{t}{t_s}\right)^{3n-3},$$

where

$$\tilde{F}(\chi_0)=\lim_{y\to 0}\tilde{F}(\chi_0,y) \tag{72}$$

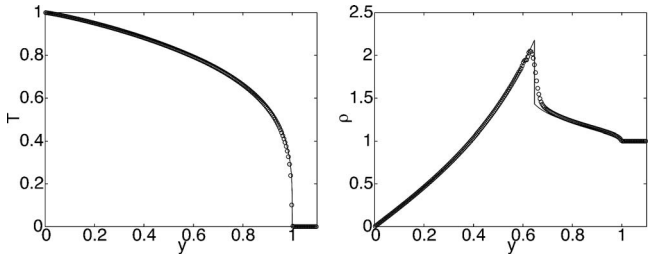

FIG. 8. Comparisons between FCI2 numerical simulations (circles) and theoretical self-similar profiles (solid lines). Here, $\chi_0=2$.

$$\tilde{F}(\chi_0,y)=\chi_0^{(1-\mu/2+\lambda)/(2-2\mu+\lambda)}\left[-\frac{1}{\Gamma}\hat{V}^{\lambda}(y)\partial_y\hat{\xi}(y)\right] \tag{73}$$

is the normalized heat flux plotted in Figs. 4–6. Remember that the profiles $\hat{\xi}$ and $\hat{V}$ and the eigenvalue Γ only depend on χ_0, which is why $\tilde{F}(\chi_0)$ only depends on χ_0. From the numerical integration of the system (51)–(54) with different $\chi_0\in[0.25,2]$, we observe a very slight decay of 3% of $\tilde{F}(\chi_0)$ when going from $\chi_0=0.25$ to $\chi_0=2$. Remember that the density dependence of the surface heat flux appears only through $\tilde{F}(\chi_0)$. This shows that the surface heat flux depends hardly on the initial density ρ_0, while the inner heat flux profiles are very sensitive toρ_0. The absorbed energy $E(t)$ satisfies $F=\partial_t E$, so that it does not depend much on the initial density either. These observations would certainly deserve a more detailed analysis, that we will not carry out in this paper.

D. Numerical simulations

We compare our analytic solutions with numerical results from the FCI2 radiation-hydrodynamics code.[15] The FCI2 settings are as follows:

- one-dimensional Lagrangian method with gray radiation diffusion,
- power-law equation of state and Rosseland opacity from Ref. 11,
- hydrodynamic boundary condition: evanescent pressure at the inner wall surface,
- radiative boundary condition: black-body flux incoming at the inner surface, with a power-law profile $T_S(t)=T_{S0}(t/t_S)^k$.

The last condition is slightly inconsistent with the analytic model, since the inner surface temperature is smaller than the incident flux temperature, due to the Milne effect. However, as soon as the radiation wave has traveled a few Rosseland mean free paths inside the wall, the two temperatures become very close to each other (data not shown).

In Fig. 7 we compare the time evolution of the temperature front and the isothermal shock, with $\chi_0=2$. In the left diagram, we display the code results, as a map of $|\partial_t(\ln\rho(t,m))|$, where t is the time in nanoseconds, and m the Lagrangian coordinate in g/cm^2. On this map both features can clearly be seen, and are in good agreement with the right diagram, showing at the same scale the results we obtained from Eqs. (48) and (50), with the eigenvalue $\Gamma=1.47$. With

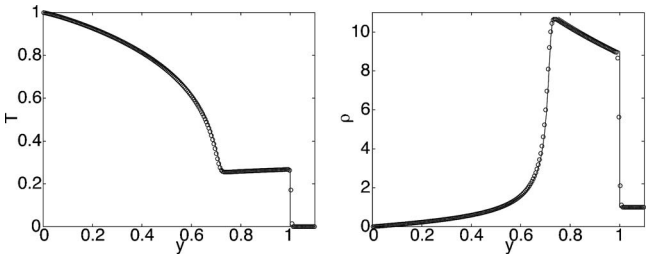

FIG. 9. Comparisons between FCI2 numerical simulations and theoretical self-similar profiles. Here, $\chi_0=0.25$.

the numerical data in (2), the time exponent n of both the temperature front and the isothermal shock is 1.348. A slight lag of the code fronts with respect to the analytic fronts is due to the above mentioned Milne effect.

In Fig. 8 we display FCI2 temperature and density spatial profiles at time 5 ns, with $k=0.4348$ (critical exponent), $T_{S0}=5\times10^6$ K, and $t_S=5$ ns. The initial density is $\rho_0=0.356$ g/cm^3, which corresponds to $\chi_0=2$. To ensure a proper analytic-numeric comparison, we normalize the FCI2 temperature to the surface temperature, and we take as $y=1$ the front location obtained by the code. The agreement is good with the analytic results. In particular, the location and strength of the isothermal shock at $y_c\simeq0.65$ are both well reproduced, even though the shock is smeared over a few cells by the numerical scheme.

In Fig. 9 we display FCI2 temperature and density spatial profiles obtained with the same numerical data, but $\rho_0=1.0515$ g/cm^3, which corresponds to $\chi_0=0.25$. The agreement is excellent with the analytic results.

V. CONCLUSION

The results in this paper describe analytical solutions of the nonlinear radiative equation when the internal energy and the opacity have power-law dependences in the density and in the temperature. In different regimes, we have exhibited locally or globally self-similar solutions that allow an exact description of the flow. In particular, we have shown that the absorbed energy as a function of the density presents a minimum. This result has been derived previously by Rosen and Hammer[12] that generalized and expanded upon the work of Hammer and Rosen,[11] which used a perturbation theory using the small parameter $\varepsilon=\beta/(4+\alpha)$, where the internal energy varies as T^β and the opacity varies as $T^{-\alpha}$. In this paper we extend the analysis to any values of α and β, we show that the flows behind the heat front are smooth, and we clarify the domain of validity of the results in terms of the imposed surface temperature. At the boundary of this domain, we have exhibited a globally self-similar solution that can be observed when the imposed surface temperature has a time power law with a critical exponent. Depending on the initial density, this self-similar flow can exhibit a heat wave followed by an isothermal shock, or a classical shock followed by an ablation front. This last configuration is the one that is typically encountered in ICF configurations. As a consequence, this exact solution could be used as a reference solution for numerical codes, or as an unperturbed one-dimensional flow for the study of the ablative Rayleigh-Taylor instability.[16–18] This idea has already been successfully applied to the linear stability of self-similar ablation flows in the case of an ideal gas.[19,20]

[1] R. E. Marshak, Phys. Fluids **1**, 24 (1958).
[2] L. Brun, R. Dautray, F. Delobeau, C. Patou, F. Perrot, J.-M. Reisse, B. Sitt, and J.-P. Watteau, in *Laser Interaction and Related Plasma Phenomena*, edited by H. J. Schwartz and H. Hora (Plenum, New York, 1977), Vol. 4, pp. 1059–1080.
[3] S. I. Anisimov, JETP Lett. **12**, 287 (1970).
[4] A. Barrero and J. R. Sanmartin, Phys. Fluids **20**, 1155 (1977).
[5] J. R. Sanmartin and A. Barrero, Phys. Fluids **21**, 1957 (1978); Phys. Fluids **21**, 1967 (1978).
[6] J. Sanz, A. R. Piriz, and F. G. Tomasel, Phys. Fluids B **4**, 683 (1992).
[7] Iu. V. Afanas'ev, V. M. Krol', O. N. Krokhin, and I. V. Nemchinov, Appl. Math. Mech. **30**, 1218 (1966).
[8] R. Pakula and R. Sigel, Phys. Fluids **28**, 232 (1985).
[9] N. Kaiser, J. Meyer-ter-Vehn, and R. Sigel, Phys. Fluids B **1**, 1747 (1989).
[10] R. Sigel, R. Pakula, S. Sakabe, and G. D. Tsakiris, Phys. Rev. A **38**, 5779 (1988).
[11] J. H. Hammer and M. D. Rosen, Phys. Plasmas **10**, 1829 (2003).
[12] M. D. Rosen and J. H. Hammer, Phys. Rev. E **72**, 056403 (2005).
[13] L. D. Landau and E. M. Lifshitz, *Fluid Mechanics* (Elsevier, Amsterdam, 2004).
[14] Ya. B. Zel'dovich and Yu. P. Rayzer, *Physics of Shock Waves and High-temperature Hydrodynamics Phenomena* (Academic, New York, 1967).
[15] E. Buresi, J. Coutant, R. Dautray, M. Decroisette, B. Duborgel, P. Guillaneux, J. Launspach, P. Nelson, C. Patou, J.-M. Reisse, and J.-P. Watteau, Laser Part. Beams **4**, 531 (1986).
[16] J. Sanz, Phys. Rev. Lett. **73**, 2700 (1994).
[17] V. N. Goncharov, R. L. Betti, R. L. McCrory, P. Sorotokin, and C. P. Verdon, Phys. Plasmas **3**, 1402 (1996).
[18] P. Clavin and L. Masse, Phys. Plasmas **11**, 690 (2004).
[19] F. Abéguilé, C. Boudesocque-Dubois, J.-M. Clarisse, S. Gautier, and Y. Saillard, Phys. Rev. Lett. **97**, 035002 (2006).
[20] J. Sanz, J. Garnier, C. Cherfils, B. Canaud, L. Masse, and M. Temporal, Phys. Plasmas **12**, 112702 (2005).